

# Increased Risk of the 2019 Alaskan July Fires due to Anthropogenic Activity

Yan Yu, John P. Dunne, Elena Shevliakova, Paul Ginoux, Sergey Malyshev, Jasmin G. John, and John P. Krasting

July 2019 saw record-breaking wildfires burning 3,600 km<sup>2</sup> in Alaska. The GFDL Earth system model indicates a threefold increased risk of Alaska's extreme fires during recent decades due to primarily anthropogenic ignition and secondarily climate-induced biofuel abundance.

**AFFILIATIONS:** Yu—Atmospheric and Oceanic Sciences Program, Princeton University, Princeton, New Jersey; Dunne, Shevliakova, Ginoux, Malyshev, John, and Krasting—NOAA Geophysical Fluid Dynamics Laboratory, Princeton, New Jersey

**CORRESPONDING AUTHOR:** Yan Yu, [yanyu@princeton.edu](mailto:yanyu@princeton.edu)

**DOI:**10.1175/BAMS-D-20-0154.1

A supplement to this article is available online ([10.1175/BAMS-D-20-0154.2](https://doi.org/10.1175/BAMS-D-20-0154.2))

©2021 American Meteorological Society  
For information regarding reuse of this content and general copyright information, consult the [AMS Copyright Policy](#).

With more than 700 wildfires and over two million acres burned in Alaska, 2019 was ranked 8th and 11th in Alaska's history in fire counts and burned area, respectively (Alaska Interagency Coordination Center 2020). Smoke plumes from July 2019 fires degraded air quality over most of Alaska, inducing the first ever dense smoke advisory (visibility less than a mile) for Anchorage, and some of the world's worst air quality in Anchorage and Fairbanks (Di Liberto 2019). Ignited by a lightning strike, the Swan Lake Fire, the most expensive fire in Alaska history, originated in the Kenai National Wildlife Refuge in southern Alaska early June and lasted for several months (Hollander 2019).

Extremely hot and dry conditions supported the unusually early and strong peak of the Alaska fire season in July 2019 (Fig. 1). Anomalous heat in spring and early sum-

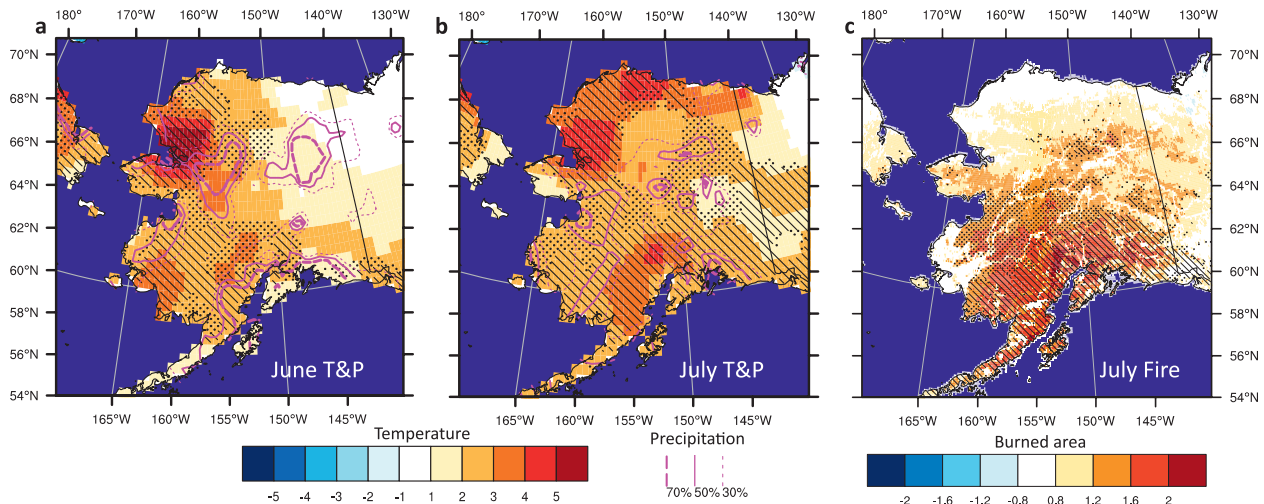


**Fig. 1. Observed meteorological conditions in Alaska during the June to July fire season in 2019.** (a),(b) Anomalies in 2-m air temperature ( $^{\circ}\text{C}$ ; color) and precipitation (contours represent 30%, 50%, and 70% lower than climatology) in (a) June and (b) July 2019, compared to the long-term average from 1979–2018. (c) Burned fraction anomalies (%) in July 2019, compared to the long-term average from 2000–18. Slashes indicate areas where the temperature in (a) and (b) or the burned fraction anomaly in (c) exceeded the highest value from the past. Stitches indicate areas where anomalies exceeded the 95th percentile in (a) and (b) and 90th percentile in (c) from the past. Analyzed datasets include National Oceanic and Atmospheric Administration (NOAA) Climate Prediction Center (CPC) Global Unified Gauge-Based Analysis of Daily temperature and precipitation (Chen et al. 2008) and MODIS burned area fraction.

mer of 2019 (Fig. 1a) and continued hot and dry conditions into July (Fig. 1b) enhanced biofuel flammability, especially over the southern and central forests in Alaska, leading to the record-breaking July burned area fraction in these regions (Fig. 1c). Indeed, 2019 saw Alaska's hottest July on record, during which its largest city, Anchorage, had a daily maximum temperature exceeding 90°F (32°C) for the first time (Di Liberto 2019). To assess the risk of extreme fires in Alaska, a previous study analyzed a Buildup Index (BUI) for potential biofuel availability and flammability, derived from cumulative scoring of daily temperature, relative humidity, and precipitation (Partain et al. 2016). Based on the BUI, Partain et al. (2016) attributed the increased risk of an extreme Alaskan fire season to anthropogenic climate change, especially warming. However, this weather-based BUI did not account for direct anthropogenic influence on fire ignition or more complex response of the land biosphere to human-induced climate change and  $\text{CO}_2$  fertilization.

Indeed, the human-induced increase in the risk of extreme fires in Alaska is also likely attributed to elevated abundance of biofuel (Liu et al. 2015) and increased number of human-ignited fires (Kasischke et al. 2010), in addition to the higher chance of biofuel drying (Pithan and Mauritsen 2014). High-latitude ecosystems such as Alaska are believed to be most vulnerable to warming under anthropogenic climate change (Pithan and Mauritsen 2014). The  $\text{CO}_2$  fertilization and excessive heat have resulted in an expansion and early-season growth of vegetation in the boreal forests (Mao et al. 2016; Liu et al. 2015), potentially causing early fuel abundance, more frequent and long-lasting fire events, and dense smoke releases, such as those seen in July 2019. Furthermore, an analysis of Alaska's fire ignition database indicated that human presence increased the number of ignitions near settlements, roads, and rivers during the past decades (Kasischke et al. 2010). These complex interactions between fire, climate, land ecosystem, and human activity, cannot be neglected in attribution studies of wildfires.

The present study takes advantage of the modeling capability of the Geophysical Fluid Dynamics Laboratory (GFDL) Earth System Model 4.1 (ESM4.1) to simulate all

these interactions in order to assess the influence of anthropogenic activities on extreme fires in Alaska. By combining ESM4.1 simulations with satellite data, we are able to evaluate the contribution of natural and anthropogenic ignition activities, anthropogenic climate variability and change, and human influence on the land ecosystem on the occurrence of extreme fire season in Alaska.

## Data and method.

To assess the influence of anthropogenic activity on the risk of extreme Alaska fire, we analyze simulations from the GFDL ESM4.1 (Dunne et al. 2020) for phase 6 of the Coupled Model Intercomparison Project (CMIP6) (Eyring et al. 2016). ESM4.1 provides coupled carbon–chemistry–climate simulations and contributes to multiple endorsed intercomparisons in CMIP6 (Eyring et al. 2016). ESM4.1 features vastly improved representation of climate mean and variability patterns from GFDL's previous chemistry and carbon coupled models (Dunne et al. 2020). The terrestrial component of ESM4.1, LM4.1 (Shevliakova et al. 2020, manuscript submitted to *J. Adv. Model. Earth Syst.*), includes a new fire model with separate data-based parameterizations for croplands and pastures (Rabin et al. 2018) and process-based parameterizations for primary and secondary lands (i.e., Fire Including Natural and Agricultural Lands model version 2, FINAL v2) (Ward et al. 2018; Rabin et al. 2018, 2015). This dynamical fire model enables representation of multi-day and crown wildfires and accounts for effects of both changes in land surface meteorological conditions and state of vegetation (Shevliakova et al. 2020, manuscript submitted to *J. Adv. Model. Earth Syst.*), thereby facilitating comprehensive projection of joint states of climate, vegetation, and fire.

The fraction of attributable risk (FAR) methodology (Stott et al. 2016) is used to examine how anthropogenic warming and ignition have changed the occurrence of an extreme fire season in Alaska, in terms of burned area and fire carbon emission. Here we analyze the risk ratio (RR) metric to quantify the factor by which the risk of an extreme event has been changed by external forcing (Fischer and Knutti 2015). To obtain such risks in the actual and natural world, lognormal cumulative distribution functions (CDFs) of Alaska's burned area and fire carbon emission in July are estimated from the time series of preindustrial and historical simulations by ESM4.1, as well as observational datasets. The Kolmogorov–Smirnov test is applied for determining the statistical significance of the difference between these CDFs (Marsaglia et al. 2003). RR is subsequently defined as  $P_{\text{historical}}/P_{\text{preindustrial}}$ , where  $P_{\text{historical}}$  is the probability of exceeding the extremeness of the observed July 2019 event in the observational CDF, and  $P_{\text{preindustrial}}$  is the probability of exceeding such extremeness in the preindustrial CDF. To account for potential model biases, the threshold value to be attributed is obtained by projecting the observed percentile of the July 2019 value in the observational distribution onto the historical distribution during 2003–19. Here the extended historical ESM4.1 time series for 1850–2019 is obtained by combining years 1850–2014 from the historical simulation (Krasting et al. 2018a) and years 2015–19 from the future projection simulation under the Shared Socioeconomic Pathway (SSP) 5–8.5 (O'Neill et al. 2016; John et al. 2018). Analyzed observational datasets for 2003–19 include burned area from the Moderate Resolution Imaging Spectroradiometer (MODIS) onboard both the *Terra* and *Aqua* satellites (Melchiorre and Boschetti 2018) and fire carbon emission from the European Center for Medium-Range Weather Forecasts (ECMWF) Copernicus Atmosphere Monitoring Service (CAMS) Global Fire Assimilation System (GFAS) (Kaiser et al. 2012). Corresponding to the observational data length, various 17-yr time windows from the 500-yr preindustrial control run time series (Krasting et al. 2018b) are utilized for the estimation of CDF and RR, thereby facilitating uncertainty quantification. In addition to the historical and preindustrial simulations, the simulation forced by 1%  $\text{yr}^{-1}$   $\text{CO}_2$  concentration increase (1pct $\text{CO}_2$ ) (Eyring et al. 2016; Krasting et al. 2018c) is analyzed for disentangling the specific anthropogenic influences on the occurrence of extreme fire season in Alaska.

## Results.

The comparison of simulated burned area and carbon emission from fires across Alaska with satellite data indicates satisfactory results with ESM4.1 (see Fig. ES1 in the supplemental material). Indeed, the historical simulation and observations of burned area and fire carbon emission consistently identify fire hotspots in the boreal forest region dominated by evergreen conifer trees in interior Alaska. Although the simulated historical burned fraction and fire carbon emission are generally smaller than observed, the model performance warrants credible attribution of the historical occurrence of an extreme fire season in Alaska.

According to ESM4.1, Alaska's July burned area and fire carbon emission increased since 1950s in ESM4.1, resulting in higher occurrence of a 2019-like event during recent decades, attributable to anthropogenic activity (Fig. 2). The probability of exceeding the burned area equivalent to the 2019 extreme fire season in Alaska increased from 2% before the 1950s to 7% after the 1950s (Fig. 2a). Furthermore, 63 out of the 100 consecutive 17-yr windows during 1850–1949 showed significant difference with 2003–19 in terms of probability distribution, whereas none of the 17-yr windows after 1950 showed significant difference with 2003–19 (Fig. 2a). The historical increase in the occurrence of an extremely fire-active July in Alaska is attributable to anthropogenic

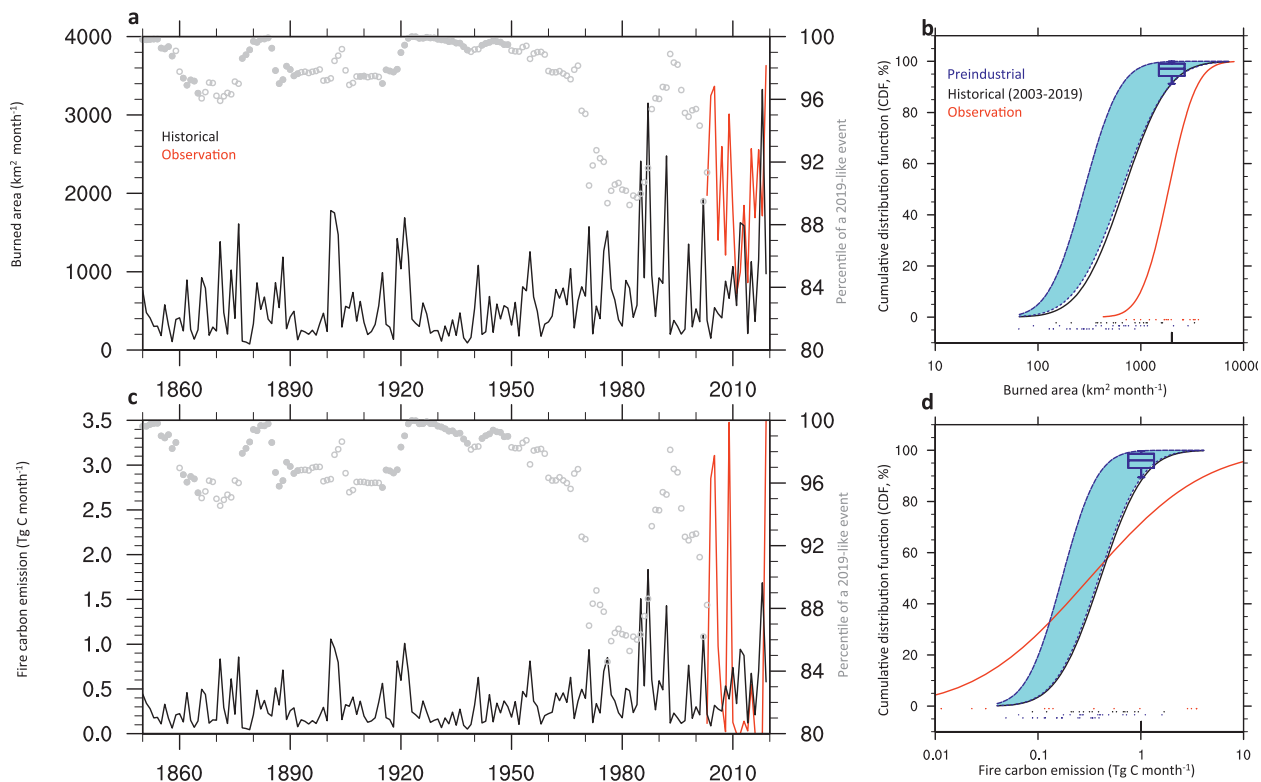


**Fig. 2. Observational, historical, and preindustrial distribution of Alaska's July fire activity.** (a),(c) Time series of Alaska's July burned area ( $\text{km}^2 \text{ month}^{-1}$ ) and fire carbon emission ( $\text{Tg C month}^{-1}$ ), respectively, from ESM4.1 (black) and observation (red), referring to the left y axis. The gray circles represent the percentile of a 2019-like event in the consecutive 17-yr window, referring to the right y axis. The filled circles indicate 17-yr periods with significantly ( $p < 0.05$ ) different distribution than 2003–19 in the ESM4.1 simulation. (b),(d) Cumulative distribution function (CDF, %) of burned area and fire carbon emission, respectively, in Alaska in July from observations (red) and ESM4.1 historical simulation (black) during 2003–19, as well as 500 years of ESM4.1 preindustrial simulation (blue). Dots indicate burned area and fire carbon emission in each sampled year from observation and each simulation. The boxplots show the 5th, 25th, 50th, 75th, and 95th percentiles of the percentile of a 2019-like event in all consecutive 17-yr windows from the preindustrial time series (sample size = 484). The uncertainty range of the preindustrial CDF is (the dashed blue curves) bounded by the CDFs derived from the 17-yr windows that produce the 5th and 95th percentiles of the percentile of a 2019-like event.

activity. In terms of burned area, 96% of the 484 preindustrial 17-yr windows show significantly different ( $p < 0.05$ ) distribution than the historical 2003–19 according to the Kolmogorov–Smirnov test. The burned area associated with a 2019-like event, namely the 91st percentile in the historical times series, is equivalent to the 97th percentile in the preindustrial time series, with a 90% confidence interval of the 92nd to 100th percentile (Fig. 2b). These CDFs result in a RR,  $P_{\text{historical}}/P_{\text{preindustrial}}$ , of 3, with a 90% confidence interval of 1.12 to infinite. The large uncertainty in the estimated RR is mainly due to the small sample size associated with the short observational record. The historical evolution and attribution of fire carbon emission were largely consistent with those of burned area across Alaska in July (Figs. 2c,d).

The historical expansion in Alaska's burned area in July was primarily caused by an increase in anthropogenic ignition, and secondarily through climate-induced biomass abundance (Fig. 3). The historical trend in burned area, approximately proportional to the product of number of fires per area ( $N_{\text{fire}}$ ) and burned area per fire ( $\text{BA}_{\text{perfire}}$ ), was mainly due to the former,  $N_{\text{fire}}$ , which exhibits a significant, positive trend ( $p < 0.001$ ) according to the Mann–Kendall trend test (Fig. 3a), whereas  $\text{BA}_{\text{perfire}}$  shows a moderate, marginally insignificant ( $p = 0.06$ ) trend (Fig. 3b). In FINAL v2 [Rabin et al. 2018, Eq. (4) therein], the evolution of  $N_{\text{fire}}$  can be further decomposed as the product of an ignition term, a direct climate factor, a climate-induced aboveground biomass factor, and an anthropogenic suppression on ignition efficiency factor ( $1 - \text{Suppression}_{\text{PD}}$ ). The ignition term includes both natural and anthropogenic components. Anthropogenic ignition includes intentional or unintentional activities, such as land and ecosystem management, smoking, railroad sparks, and power lines (Fusco et al. 2016), and is represented as a function of population density in FINAL v2 (Rabin et al. 2018). Between 48% and 86% of the observed fires in Alaska were caused by anthropogenic ignition in the recent decade

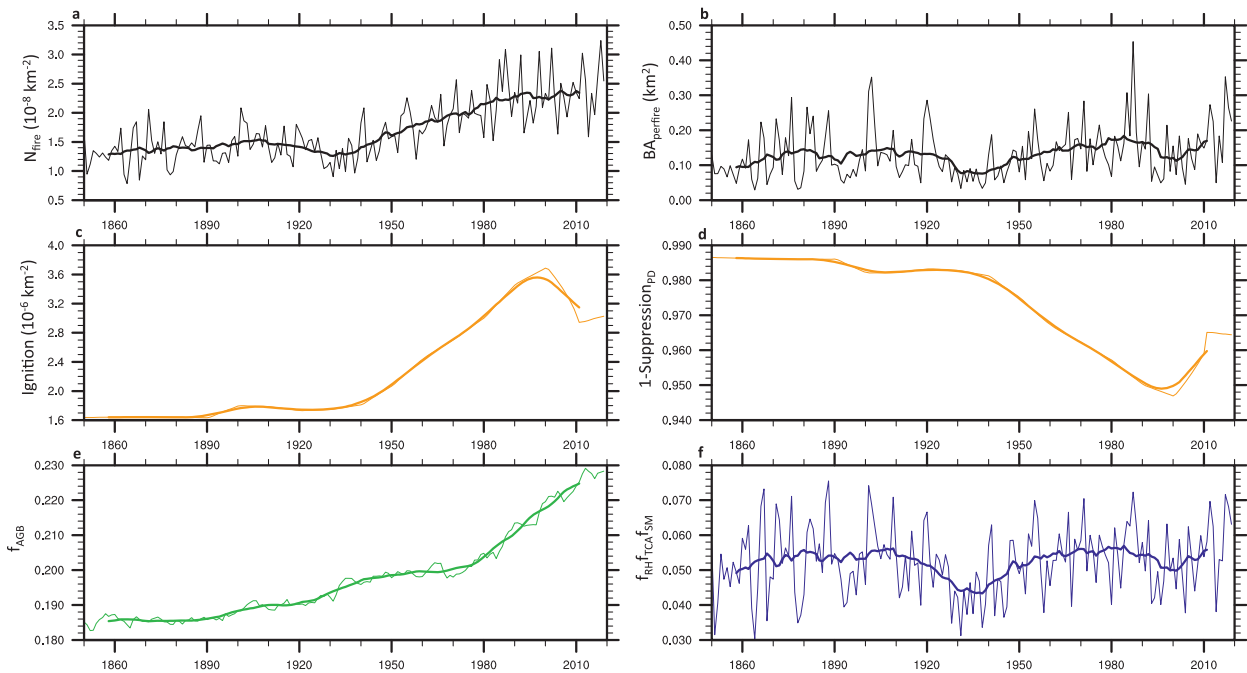


**Fig. 3.** Time series of Alaska's fire number, size, and contributing factors in July during 1850–2019, from the ESM4.1 historical simulation. The analyzed variables include (a) the number of fires per area ( $10^{-8} \text{ km}^{-2}$ ), (b) the burned area per fire ( $\text{km}^2$ ), (c) total ignitions ( $10^{-6} \text{ km}^{-2}$ ), (d) the function of population density, expressed as unity subtracted by human-induced suppression on fire number, (e) the function of aboveground biomass (unitless), and (f) the product of the function of relative humidity, canopy air temperature, and soil moisture. In ESM4.1, number of fires per area is calculated by multiplying the factors shown in (c)–(f). The thick lines represent the 17-yr running average.

(Alaska Interagency Coordination Center 2020). Given the input of an invariant seasonal cycle of lightning to FINAL, the temporal variation in ignition is controlled by anthropogenic ignition. The historical  $N_{\text{fire}}$  increased from  $1.2 \times 10^{-8} \text{ km}^{-2}$  during 1850–66 to  $2.4 \times 10^{-8} \text{ km}^{-2}$  during 2003–19. Based on the decomposition, this twofold increase in  $N_{\text{fire}}$  was primarily driven by the trend in anthropogenic ignition, as the total ignition intensity increased from  $1.6 \times 10^{-6} \text{ km}^{-2}$  during 1850–66 to  $2.9 \times 10^{-6} \text{ km}^{-2}$ , out of which 62% were caused by anthropogenic ignition, during 2003–19. Although increased population density also resulted in elevated human suppression on ignition efficiency (Fig. 3d), this  $1 - \text{Suppression}_{\text{PD}}$  term decreased only slightly from 0.986 during 1850–66 to 0.948 during 2003–19, because of the moderate population density in Alaska. A secondary contribution came from the climate-induced abundance in aboveground biomass, whose contributing factor increased from 0.19 during 1850–66 to 0.22 during 2003–19. Direct influence of anthropogenic climate change on weather patterns appeared to play a minor role in the historical increase of  $N_{\text{fire}}$  in Alaska in July. As a further evidence of the key influence of climate-induced biofuel abundance on the historically increased number of fires in Alaska, the 1pctCO<sub>2</sub> experiment, which does not involve changes in anthropogenic ignition or anthropogenic suppression on ignition efficiency, shows comparable relative increase in fire carbon emission and the contribution from climate-induced biofuel abundance during the simulated 150 years (Fig. ES2).

## Conclusions and discussion.

July 2019 saw record-breaking wildfires that burned over 3,600 km<sup>2</sup> and emitted an estimate of 3.5 Tg of carbon in Alaska, accompanied by extremely hot and dry conditions in June and July. According to GFDL ESM4.1, in July burned area and fire carbon emission increased since 1950s in Alaska, resulting in higher occurrence of a 2019-like event during recent decades. The historical increase in the occurrence of an extremely fire-active July was attributed to anthropogenic activity, which caused a threefold increase in the risk of a 2019-like fire season. The anthropogenic influence on the increased occurrence of an extreme fire season in Alaska was primarily through an increase in anthropogenic ignition, and secondarily through climate-induced biomass abundance.

A limitation of our analysis is the use of a single Earth system model, thereby introducing uncertainty in the detection and attribution of an extreme fire season in Alaska. For example, the historical ESM4.1 simulation features a general underestimation of both burned area and fire carbon emission across Alaska (Fig. ES1), unrealistic representation of observed year-to-year variations in regional burned area (Fig. 2a), and a narrower distribution of the historical, regional fire carbon emission (Figs. 2c,d). This model bias is potentially caused by underrepresentation of the trends and interannual variability in fire ignition due to lightning (Rabin et al. 2018). Although this apparent model bias is partially accounted for in the analysis, its quantitative influence on the RR remains unclear. Another possible bias is the inconsistent modeling of radiative impact of aerosols from fires. The model is based on CMIP6 emission inventory rather than using the injected aerosols from the simulated fires to calculate the radiative forcing. Other factors that are not included in the model may further complicate the human–ecosystem–fire interactions. For example, ESM4.1 does not include changing tree mortality from beetles that might also drive changes in fire spread (Hicke et al. 2012). To quantify the uncertainties introduced by analyzing a single model ESM4.1, future studies are encouraged to expand the current analysis to multiple Earth system models that represent fire dynamics.

**Acknowledgments.** This research is supported by NOAA and Princeton University's Cooperative Institute for Climate Science. The authors thank Isabel Martínez Cano and Khaled Ghannam for their helpful comments on the early version of this paper. The comments from two reviewers were greatly appreciated.

## References

Alaska Interagency Coordination Center, 2020: Alaska fire numbers 2019. Accessed 6 April 2020, <https://fire.ak.blm.gov/content/aicc/Statistics%20Directory/Previous%20Years%20Data%20and%20FFR%20Handouts/2019%20Fire%20Data/Alaska%20Fire%20Season%2019%20Presentation.pdf>.

Chen, M., W. Shi, P. Xie, V. B. S. Silva, V. E. Kousky, R. W. Higgins, and J. E. Janowiak, 2008: Assessing objective techniques for gauge-based analyses of global daily precipitation. *J. Geophys. Res.*, **113**, D04110, <https://doi.org/10.1029/2007JD009132>.

Di Liberto, T., 2019: High temperatures smash all-time records in Alaska in early July 2019. NOAA, Accessed 6 April 2020, <https://www.climate.gov/news-features/event-tracker/high-temperatures-smash-all-time-records-alaska-early-july-2019>.

Dunne, J. P., and Coauthors, 2020: The GFDL Earth System Model version 4.1 (GFDL-ESM 4.1): Overall coupled model description and simulation characteristics. *J. Adv. Model. Earth Syst.*, <https://doi.org/10.1029/2019MS002015>, in press.

Eyring, V., S. Bony, G. A. Meehl, C. A. Senior, B. Stevens, R. J. Stouffer, and K. E. Taylor, 2016: Overview of the Coupled Model Intercomparison Project Phase 6 (CMIP6) experimental design and organization. *Geosci. Model Dev.*, **9**, 1937–1958, <https://doi.org/10.5194/gmd-9-1937-2016>.

Fischer, E. M., and R. Knutti, 2015: Anthropogenic contribution to global occurrence of heavy-precipitation and high-temperature extremes. *Nat. Climate Change*, **5**, 560–564, <https://doi.org/10.1038/nclimate2617>.

Fusco, E. J., J. T. Abatzoglou, J. K. Balch, J. T. Finn, and B. A. Bradley, 2016: Quantifying the human influence on fire ignition across the western USA. *Ecol. Appl.*, **26**, 2390–2401, <https://doi.org/10.1002/eap.1395>.

Hicke, J. A., M. C. Johnson, J. L. Hayes, and H. K. Preisler, 2012: Effects of bark beetle–caused tree mortality on wildfire. *For. Ecol. Manage.*, **271**, 81–90, <https://doi.org/10.1016/j.foreco.2012.02.005>.

Hollander, Z., 2019: An Alaska wildfire is the nation's most expensive so far this season. <https://www.adn.com/alaska-news/2019/09/19/an-alaskan-wildfire-is-the-nations-most-expensive-so-far-this-season/>.

John, J. G., and Coauthors, 2018: NOAA-GFDL GFDL-ESM4 model output prepared for CMIP6 ScenarioMIP ssp585. Earth System Grid Federation, accessed 27 January 2020, <https://doi.org/10.22033/ESGF/CMIP6.8706>.

Kaiser, J. W., and Coauthors, 2012: Biomass burning emissions estimated with a global fire assimilation system based on observed fire radiative power. *Biogeosciences*, **9**, 527–554, <https://doi.org/10.5194/bg-9-527-2012>.

Kasischke, E. S., and Coauthors, 2010: Alaska's changing fire regime—Implications for the vulnerability of its boreal forests. *Can. J. For. Res.*, **40**, 1313–1324, <https://doi.org/10.1139/X10-098>.

Krasting, J. P., and Coauthors, 2018a: NOAA-GFDL GFDL-ESM4 model output prepared for CMIP6 CMIP historical. Earth System Grid Federation, accessed 27 January 2020, <https://doi.org/10.22033/ESGF/CMIP6.8597>.

Krasting, J. P., and Coauthors, 2018b: NOAA-GFDL GFDL-ESM4 model output prepared for CMIP6 CMIP piControl. Earth System Grid Federation, accessed 27 January 2020, <https://doi.org/10.22033/ESGF/CMIP6.8669>.

Krasting, J. P., and Coauthors, 2018c: NOAA-GFDL GFDL-ESM4 model output prepared for CMIP6 CMIP 1pctCO2. Earth System Grid Federation, accessed 27 January 2020, <https://doi.org/10.22033/ESGF/CMIP6.8473>.

Liu, Y. Y., A. I. J. M. van Dijk, R. A. M. de Jeu, J. G. Canadell, M. F. McCabe, J. P. Evans, and G. Wang, 2015: Recent reversal in loss of global terrestrial biomass. *Nat. Climate Change*, **5**, 470–474, <https://doi.org/10.1038/nclimate2581>.

Mao, J., and Coauthors, 2016: Human-induced greening of the northern extratropical land surface. *Nat. Climate Change*, **6**, 959–963, <https://doi.org/10.1038/nclimate3056>.

Marsaglia, G., W. W. Tsang, and J. Wang, 2003: Evaluating Kolmogorov's distribution. *J. Stat. Software*, **8** (18), 1–4, <https://doi.org/10.18637/jss.v008.i18>.

Melchiorre, A., and L. Boschetti, 2018: Global analysis of burned area persistence time with MODIS data. *Remote Sens.*, **10**, 750, <https://doi.org/10.3390/rs10050750>.

O'Neill, B. C., and Coauthors, 2016: The Scenario Model Intercomparison Project (ScenarioMIP) for CMIP6. *Geosci. Model Dev.*, **9**, 3461–3482, <https://doi.org/10.5194/gmd-9-3461-2016>.

Partain, J. L., Jr., and Coauthors, 2016: An assessment of the role of anthropogenic climate change in the Alaska fire season of 2015. *Bull. Amer. Meteor. Soc.*, **97**, S14–S18, <https://doi.org/10.1175/BAMS-D-16-0149.1>.

Pithan, F., and T. Mauritsen, 2014: Arctic amplification dominated by temperature feedbacks in contemporary climate models. *Nat. Geosci.*, **7**, 181–184, <https://doi.org/10.1038/ngeo2071>.

Rabin, S. S., B. I. Magi, E. Shevliakova, and S. W. Pacala, 2015: Quantifying regional, time-varying effects of cropland and pasture on vegetation fire. *Biogeosciences*, **12**, 6591–6604, <https://doi.org/10.5194/bg-12-6591-2015>.

Rabin, S. S., D. S. Ward, S. L. Malyshev, B. I. Magi, E. Shevliakova, and S. W. Pacala, 2018: A fire model with distinct crop, pasture, and non-agricultural burning: Use of new data and a model-fitting algorithm for FINAL1. *Geosci. Model Dev.*, **11**, 815–842, <https://doi.org/10.5194/gmd-11-815-2018>.

Stott, P. A., and Coauthors, 2016: Attribution of extreme weather and climate-related events. *Wiley Interdiscip. Rev.: Climate Change*, **7**, 23–41, <https://doi.org/10.1002/wcc.380>.

Ward, D. S., E. Shevliakova, S. Malyshev, and S. Rabin, 2018: Trends and variability of global fire emissions due to historical anthropogenic activities. *Global Biogeochem. Cycles*, **32**, 122–142, <https://doi.org/10.1002/2017GB005787>.